macromol

MDPI

Article

Toughened Bio-Polyamide 11 for Impact-Resistant Intraply Basalt/Flax Hybrid Composites

Claudia Sergi [1,*], Libera Vitiello [2], Pietro Russo [3], Jacopo Tirillò [1] and Fabrizio Sarasini [1]

[1] Department of Chemical Engineering Materials Environment, Sapienza Università di Roma and UdR INSTM, 00184 Rome, Italy; jacopo.tirillo@uniroma1.it (J.T.); fabrizio.sarasini@uniroma1.it (F.S.)
[2] Department of Chemical, Materials and Production Engineering, University of Naples Federico II, 80125 Naples, Italy; libera.vitiello@unina.it
[3] Institute for Polymers, Composites and Biomaterials—National Council of Research, 80078 Pozzuoli, Naples, Italy; pietro.russo@ipcb.cnr.it
* Correspondence: claudia.sergi@uniroma1.it; Tel.: +39-064-458-5647

Abstract: The automotive sector covers almost 40% of polyamide (PA) total demand. A suitable solution to improve the sustainability of this sector is the exploitation of PA matrices sourced from renewable origins, such as PA11, and their reinforcement with natural fibers such as vegetable flax and mineral basalt. A preliminary study on the quasi-static properties of PA11-based composites reinforced with an intraply flax/basalt hybrid fabric demonstrated their feasibility for semi-structural purposes in the transportation field, but their application needs to be validated against dynamic loading. In this regard, this work investigated the low-velocity impact performance of PA11 flax/basalt hybrid composites (10 J, 20 J and 30 J) as a function of temperature (room temperature and +80 °C) and plasticizer addition (butyl-benzene-sulfonamide). The results proved that plasticized PA11 is endowed with a lower glass transition temperature (~15 °C, from DMA) and melting temperature (~10 °C, from DSC), which simplifies manufacturing and processing, but also possesses a higher toughness which delays penetration phenomena and reduces permanent indentation at room temperature between 20.5% and 42.8% depending on impact energy. The occurrence of matrix plasticization at +80 °C caused a more flexible and tougher response from the laminates with a decrease in linear stiffness and a delay in penetration phenomena which made the plasticizer effect less prominent.

Keywords: polyamide 11; basalt; flax; plasticizer; low-velocity impact; polymer matrix composites; hybrid composites

Citation: Sergi, C.; Vitiello, L.; Russo, P.; Tirillò, J.; Sarasini, F. Toughened Bio-Polyamide 11 for Impact-Resistant Intraply Basalt/Flax Hybrid Composites. *Macromol* **2022**, 2, 154–167. https://doi.org/10.3390/macromol2020010

Academic Editor: Ana María Díez-Pascual

Received: 1 March 2022
Accepted: 29 March 2022
Published: 6 April 2022

1. Introduction

According to the data reported by Plastics Europe [1], 367 million tons of plastics were produced all over the world in 2020, and 15% of them, i.e., 55 million tons, were meant to cover the European demand. In total, 8.8% of this amount was absorbed by the automotive sector, which takes advantage of plastics and fiber-reinforced polymers (FRP) to achieve good mechanical performance while reducing vehicle weight and the related fuel consumption. In particular, this industrial field covers almost 40% of the total demand for polyamide (PA) engineering plastics [2].

The introduction of new European environmental regulations, apt to encourage the reduction of products' carbon footprint, caused severe issues to the automotive sector due to its extensive consumption of polymers. The first solution to this problem was given by the introduction of eco-sustainable thermoplastic polymers such as the PA11 Rilsan, which is obtained from renewable origins being synthesized from castor oil [3]. In particular, PA11 has mechanical properties slightly lower than PA12, which, on the contrary, is totally petroleum-based with a $kgCO_{2eq}/kg$ of 6.9, 40% higher than PA11 [4].

A further way to comply with the more restrictive regulations is the direct exploitation of natural materials, such as vegetable fibers, to produce fiber-reinforced polymer compos-

ites. This idea was first promoted by Henry Ford in the 1930s–1940s when he launched the hemp body car which was further developed over the last two decades [5–8]. Vegetable fibers have a lot of advantages such as renewable origin, biodegradability, high specific stiffness, low density and low cost, [9] and ensure a reduction of 20% in cost and 30% in weight of automotive components, thus leading to a decrease in fuel consumption and greenhouse gas emission [10]. Moreover, their production phase has a lower environmental impact with respect to commonly used glass fibers. For example, the production of 1 kg of hemp fibers causes emissions of 0.64 kg of CO_2, 1.2 kg of SO_x and 0.95 kg of NO_x, which are significantly lower than the 20.4 kg of CO_2, 8.8 kg of SO_x and 2.9 kg of NO_x connected with glass fiber manufacturing [11]. Their major drawback is that they are not able to ensure the same mechanical performance achievable with glass fibers when embedded in the polymer matrix. This is due to their inherently lower absolute mechanical properties compared to glass fibers and to the poor interfacial adhesion with hydrophobic polymer matrices.

Hybridization, i.e., composite materials produced with two or more reinforcements in the same matrix, is a suitable way to overcome this issue by exploiting the synergistic effect of two different reinforcements, allowing us to obtain composites with satisfying mechanical properties but with a lower weight, costs and higher environmental sustainability. Many studies have already proven the feasibility of glass and vegetable fiber hybridization [12–14], but a further step towards more eco-friendly components can be taken by replacing synthetic glass fibers with basalt ones. Basalt is a mineral natural fiber of volcanic origin which displays mechanical properties perfectly comparable with glass ones [15] and is characterized by easier recycling and recovery at the end of the composite life cycle while ensuring a reduction in the chemicals necessary to produce the reinforcement. Even in this case, many studies legitimated basalt hybridization feasibility with flax [16–18], jute [19,20] and hemp [21,22].

The present work couples these three strategies to propose a sustainable composite for automotive applications; in particular, a basalt/flax intraply fabric was employed as reinforcement in a PA11 Rilsan matrix. Some studies have already implemented hybridization with biopolyamide. Bazan et al. [23] studied the influence of basalt/aramid fibers on a biopolyamide 10.10, while Armioun et al. [24] investigated the hybridization of wood and carbon fibers in a PA11 Rilsan matrix. Recently, Russo et al. [25] performed a preliminary investigation of the composite configuration proposed in the present work, addressing the effect of plasticizer on the quasi-static properties of the neat matrix and the overall composite. In their work, Russo et al. concluded that the PA11 Rilsan matrix reinforced with the intraply basalt/flax fabric could be suitably exploited for semi-structural purposes in the transportation field, e.g., paneling. Even if some results on the impact behavior of these structures were provided as Charpy tests, it is necessary to further investigate their dynamic response to legitimate their suitability to the automotive field.

In this framework, this study focused, for the first time, on the impact performance of the bio-polyamide 11 reinforced with the hybrid flax/basalt interwoven fabric, assessing the effect of impact energy, temperature and toughness induced by matrix plasticization. The latter aspect is crucial from the impact perspective at room temperature due to the brittle response of the polymeric matrix, which is working below its glass transition temperature. The impact campaign was supported by a post-impact analysis to quantify damage extent as a function of impact energy, temperature and plasticizer addition and also by thermal analyses to disclose the effect of operating temperature on the mechanical response of the material under study.

2. Materials and Methods

2.1. Materials and Composite Manufacturing

Two different polyamides 11 (PA11) Besno Rilsan®, provided by Arkema S.A. (Puteaux, France), were used as a matrix to manufacture the composites. In particular, a PA11 (TL) with a density of 1.03 g/cm^3 and a PA11 (P40), plasticized by the inclusion of butyl-benzene-sulfonamide (BBSA), with a density of 1.04 g/cm^3 were selected. Polymeric

matrices were reinforced with an interwoven flax/basalt hybrid twill 2/2 provided by Lincore® (Bourguebus, France) with an areal density of 360 g/m^2.

The laminates were produced by hot compression molding through a P400E molding machine supplied by Collin GmbH (Ebersberg, Germany), applying the film stacking technique. In particular, each of the 10 plies of fabric was interleaved with 3 polymeric layers, and the outer fabrics were covered with 2 layers of polymers each. The complete stacking sequence is shown in Figure 1. Polymeric films with a thickness of 85 µm were produced with a Teach-Line E20T flat die extruder equipped with a CR72T calender (Collin GmbH, Ebersberg, Germany) employing a 60-rpm screw speed and a temperature profile of 170–210–220–220–200 °C. Compression molding was carried out in accordance with a pre-optimized cycle already described in [25], with a maximum temperature of 225 °C and a maximum pressure of 3 MPa. All polymeric films were dried in a vacuum at 70 °C for 12 h before hot compression. The final composite consists of 10 fabric plies, 31 polymeric films, an average thickness of 4 mm and a fiber volume fraction of 0.35.

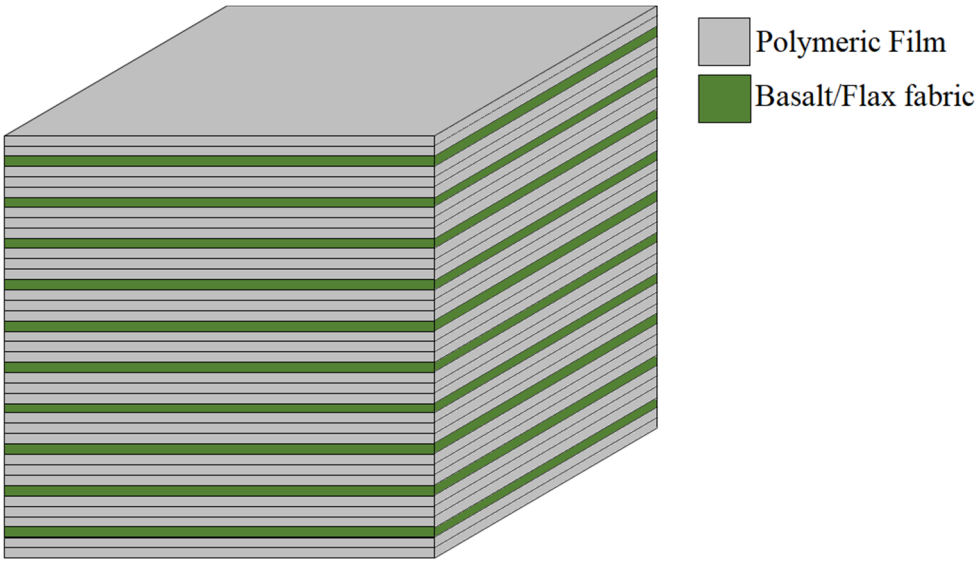

Figure 1. Stacking sequence used to produce the bio-polyamide composites.

2.2. Preliminary Thermal and Structural Characterizations

Thermal and microstructural characterizations were carried out to support PA11 impact response data interpretation. Thermogravimetric analysis (TGA), differential scanning calorimetry (DSC) and dynamic mechanical analysis (DMA) were employed to perform the thermal characterization, while X-ray diffraction (XRD) was used for structural characterization. Three samples for each configuration and each characterization technique were tested.

TGA was carried out according to ISO11358 on both composites and neat matrices in a Q500 machine supplied by TA Instruments (New Castle, DE, USA) using a heating ramp of 10 °C/min up to 700 °C in a nitrogen atmosphere. DSC was performed according to ISO11357 on PA11_TL and PA11_P40 composites with a DSC 214 Polyma by Netzsch (Selb, Germany), employing a heating and cooling ramp of 10 °C/min from −30 °C to 220 °C in a nitrogen atmosphere. DMA was conducted according to ISO 6721 with a DMA 242 E Artemis by Netzsch (Selb, Germany) in a 3-point bending configuration from −30 °C to 130 °C using a heating ramp of 2 °C/min and a frequency of 1 Hz. Finally, XRD analysis was carried out through a Philips X'Pert PRO (Almelo, Netherlands) diffractometer collecting the spectra in the range of 2θ = 10–40° with a step size of 0.02° and a time per step of 3 s employing $Cu_{k\alpha}$ monochromatic radiation (40 kV–40 mA).

2.3. Impact and Post-Impact Analysis: Low-Velocity Impacts and Profilometry

Low-velocity impact tests were carried out according to ASTM D5628 on PA11 plasticized and non-plasticized composites with an instrumented drop weight tower Instron/Ceast 9340 (Instron, Pianezza, Italy). Rectangular samples with a size of 100 mm × 150 mm were impacted at 10 J, 20 J and 30 J with a hemispherical impactor of 12.7 mm diameter and an overall mass of 8.055 kg. The sample holder was a circular hollow support with an inner diameter of 40 mm, which clamped the specimen through a pneumatic system. The tower was also equipped with an anti-rebound system that blocked the impactor after the first rebound, preventing a second impact. Tests were carried out at room temperature and +80 °C after conditioning the specimens for two hours at the desired operating temperature. Three samples for each composite configuration and each impact condition were tested. A profilometric post-impact analysis was performed with a laser profilometer (scan speed of 8500 μm/s) Talyscan 150 by Taylor Hobson (Leicester, UK) to quantify the residual indentation depth left by the impactor. The resulting scanned images were analyzed through the software TalyMap 3D.

3. Results and Discussion

3.1. Preliminary Characterization

3.1.1. TGA

The thermal stability of neat matrices and composites was investigated by TGA, and the resulting weight and derivative curves as a function of temperature are shown in Figure 2. PA11_TL displays a single degradation step at 408.35 °C coherent with the data by Oliver-Ortega et al. [26], who reported the onset temperature for 5 wt% loss of PA11 Rilsan at 409 °C. On the contrary, plasticized PA11_P40 shows two degradation stages at 233 °C and 427 °C. The second weight drop must be ascribed to PA11 degradation, while the first drop of 14% is due to plasticizer degradation, as also confirmed by Ambrósio et al. [27], who detected a mass loss of 13% between 180 °C and 420 °C as a consequence of butyl-benzene-sulfonamide (BBSA) plasticizer degradation.

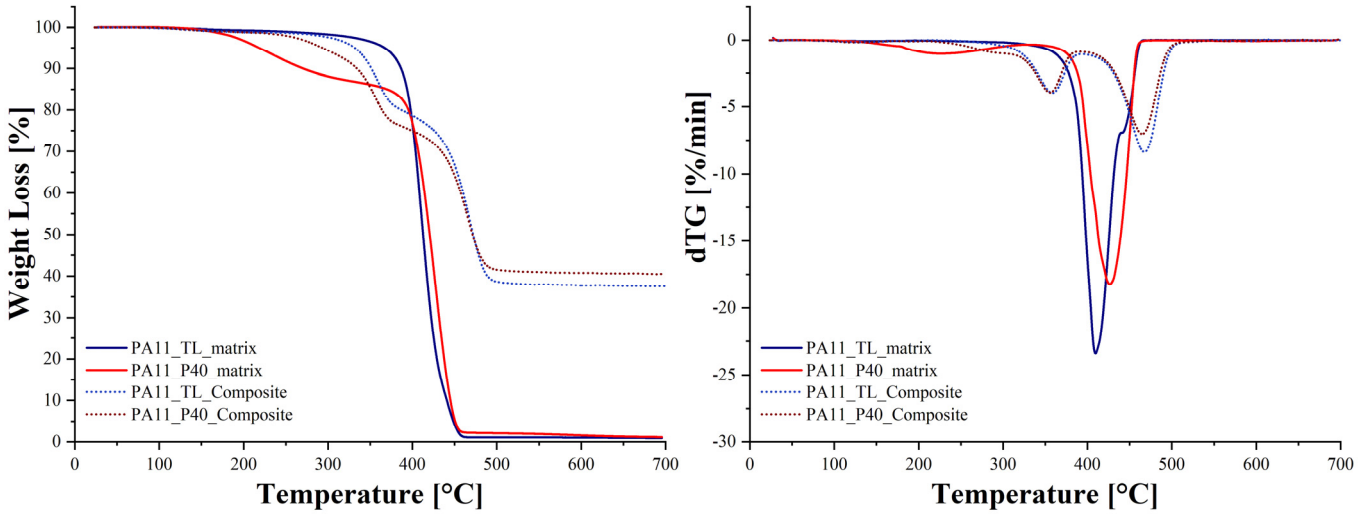

Figure 2. Weight loss and derivative curves of PA11_TL and PA11_P40 matrices and the resulting composites.

The thermal degradation analysis of the composites confirmed these results, featuring a weight drop at 467 °C for PA11_TL and two weight drops at 262 °C and 465 °C for PA11_P40. Even in this case, as already seen for the neat matrices, PA11_P40 composites' thermal degradation starts earlier than PA11_TL composites due to the presence of plasticizer, which degrades at lower temperatures. The shift of these drops towards higher temperatures can be ascribed to basalt fibers which are not sensitive to thermal degradation in this temperature range. In particular, the inert nature of basalt allows us to improve composite thermal stability, as already proved by Adole et al. [28] for high-density polyethylene

(HDPE) and by Wang et al. [29] for polypropylene (PP). Finally, both composites display a relevant mass loss of almost 18% at around 355 °C due to the degradation of cellulose and hemicellulose of flax fibers. These results agree with the ones by Kandemir et al. [30], who reported 325 °C as the flax degradation temperature, Kannan et al. [31], who provided a degradation range of 333–375 °C and by Lafranche et al. [32], who detected flax degradation at 365 °C.

3.1.2. DSC and XRD

It was possible to evaluate the main thermal properties, i.e., melting and crystallization temperatures, of both PA11_TL and PA11_P40 composites through DSC analysis. In particular, Figure 3 shows the DSC curves of both composites, while Table 1 summarizes the main parameters. Both matrices are characterized by a double melting peak due to the presence of two types of crystalline phases which lead to a two-phase transition [33]. This is confirmed by the XRD spectra reported in Figure 4, where two different peaks can be observed at 20.4° and 22.7° for PA11_TL and 20.2° and 22.8° for PA11_P40. In the literature, it is reported that the (200) plane of the triclinic α structure appears at 20° while the (010) and (210) planes appear at 23.3–23.5° [34,35]. Moreover, the (100) plane of the α′ structure, which is a pseudohexagonal δ phase, appears at 21° [36]. The occurrence of α and δ phase angles in such a short range explains why the two peaks are not perfectly well-defined. In any case, the detection of the two peaks in the XRD spectra related to the two crystalline phases allows us to justify the two-stage melting observed in DSC. Moreover, from the XRD spectra, two other peaks at 14.8° and 16.6° can be detected, and they must be ascribed to the cellulose I crystalline component deriving from flax fibers, as also confirmed by the as-received fabric spectrum, which does not show the shoulder observed at around 20°, typical of the PA11 matrix [37]. In addition, crystalline cellulose I also displays a strong diffraction peak between 22° and 22.8°, which further masks the PA11 peaks.

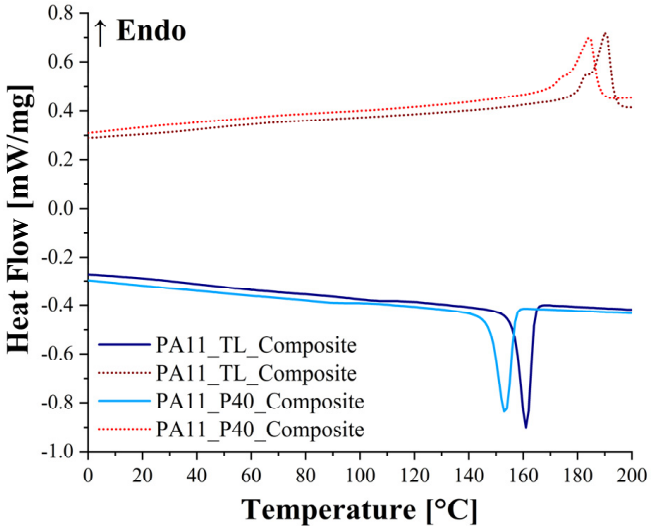

Figure 3. DSC cooling and second heating curves of PA11_TL and PA11_P40 composites.

Table 1. Crystallization and melting temperatures of PA11_TL and PA11_P40 composites.

	T_c (°C)	T_{m_lower} (°C)	T_{m_higher} (°C)
PA11_TL_Composite	161.0 ± 0.1	182.8 ±0.3	190.6 ± 0.2
PA11_P40_Composite	153.3 ± 0.1	172.1 ± 1.3	184.1 ± 0.2

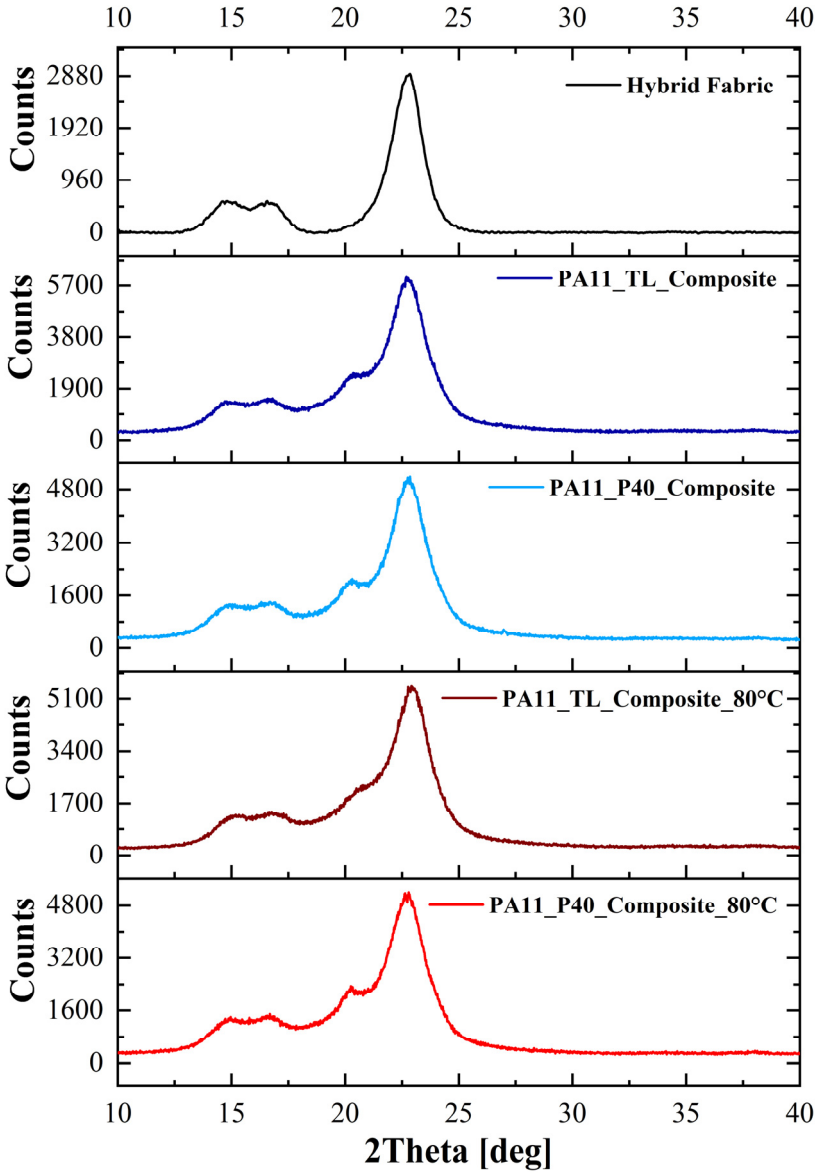

Figure 4. XRD spectra of the as-received fabric and of PA11_TL and PA11_P40 composites as-received and after exposure for 2 h at 80 °C.

Concerning the thermal analysis results, plasticized PA11_P40 composite is characterized by a decrease between 5 °C and 10 °C in melting and crystallization temperatures with respect to the PA11_TL composite, respectively, in agreement with the data reported by Russo et al. [25] for the neat matrices, meaning that no significant effects of fiber reinforcements can be detected.

3.1.3. DMA

The glass transition temperatures of plasticized and non-plasticized PA11-based composites were evaluated through the DMA curves shown in Figure 5, and the resulting data are summarized in Table 2. The glass transition temperature values evaluated at the tanδ peak are the highest ones and are consistent with the ones reported by Russo et al. [25] from DSC tests for the neat matrices, i.e., 50.5 °C for PA11_TL and 37.7 °C for PA11_P40. This huge difference in glass transition temperatures is due to the plasticizer, which not only increases PA11 flexibility at room temperature but also affects the matrix temperature response, as already detected for the melting and crystallization temperatures. The introduction of Butyl-Benzene-Sulfonamide plasticizer in the PA11 matrix causes the disruption

of the hydrogen bonds between amide groups creating stronger hydrogen bonds with them [38,39]. This leads to easier macromolecules separation and slipping, thus decreasing polymer glass transition and melting temperature.

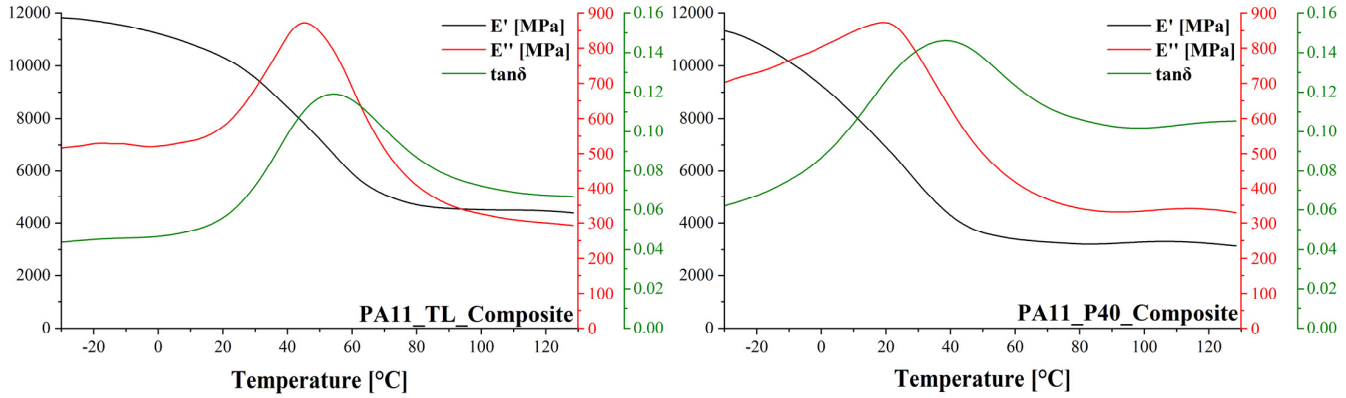

Figure 5. DMA curves of PA11_TL and PA11_P40 composites.

Table 2. Glass transition temperatures and E′ progression as a function of the temperature of PA11 plasticized and non-plasticized composites.

	$T_{g\_tan\delta}$ (°C)	E′ @ −20 °C (MPa)	E′ @ 0 °C (MPa)	E′ @ 20 °C (MPa)	E′ @ 40 °C (MPa)	E′ @ 60 °C (MPa)
PA11_TL_Composite	55.2 ± 0.3	11,723.8 ± 8.3	11,225.1 ± 12.3	10,329.8 ± 21.3	8441.7 ± 41.2	5924.4 ± 40.4
PA11_P40_Composite	39.8 ± 0.5	10,884.6 ± 20.8	9220.1 ± 35.4	6936.4 ± 44.2	4306.1 ± 34.3	3394.9 ± 5.8

3.2. Low-Velocity Impacts

As reported in the previous section, the Butyl-Benzene-Sulfonamide plasticizer breaks the hydrogen bonds between amide groups in PA11, making macromolecules slip easier. This phenomenon has a significant effect not only on the PA11 temperature response but also on its mechanical behavior. Focusing on the dynamic response, the impact curves of plasticized and non-plasticized PA11 composites at room temperature are reported in Figure 6, while the main impact parameters are summarized in Table 3. According to the glass transition temperatures calculated through DMA, i.e., 55.2 °C for PA11_TL and 39.8 °C for PA11_P40, both composite configurations work in the glassy state when impacted at room temperature. This implies a brittle response of the laminates towards the impact event. Considering this, the toughening effect of the plasticizer is fundamental to determine a more compliant response of the composite, as confirmed by the lower initial curve slope, with a decrease between 2.7% and 5.9% in peak force and an increase between 7.9% and 9.3% in maximum displacement for 10 J and 20 J, respectively. The improved toughness of PA11_P40 over PA11_TL is even more evident at 30 J, where non-plasticized PA11 experiences severe impactor penetration while the plasticized laminate displays only an initial penetration which is also delayed in terms of maximum displacement with respect to PA11_TL.

Table 3. Main impact parameters, i.e., peak force, maximum displacement and damage degree, of PA11 composites at room temperature.

	Peak Force [N]	Max. Displacement [mm]	Damage Degree
PA11_TL_Composite_10J	4257.17 ± 23.84	4.00 ± 0.04	0.67 ± 0.01
PA11_P40_Composite_10J	4004.27 ± 44.40	4.41 ± 0.10	0.69 ± 0.01
PA11_TL_Composite_20J	5657.17 ± 27.50	5.86 ± 0.01	0.79 ± 0.01
PA11_P40_Composite_20J	5503.34 ± 215.42	6.36 ± 0.18	0.74 ± 0.03
PA11_TL_Composite_30J	6044.50 ± 247.95	9.73 ± 0.95	0.97 ± 0.01
PA11_P40_Composite_30J	6081.62 ± 270.55	8.79 ± 1.01	0.93 ± 0.03

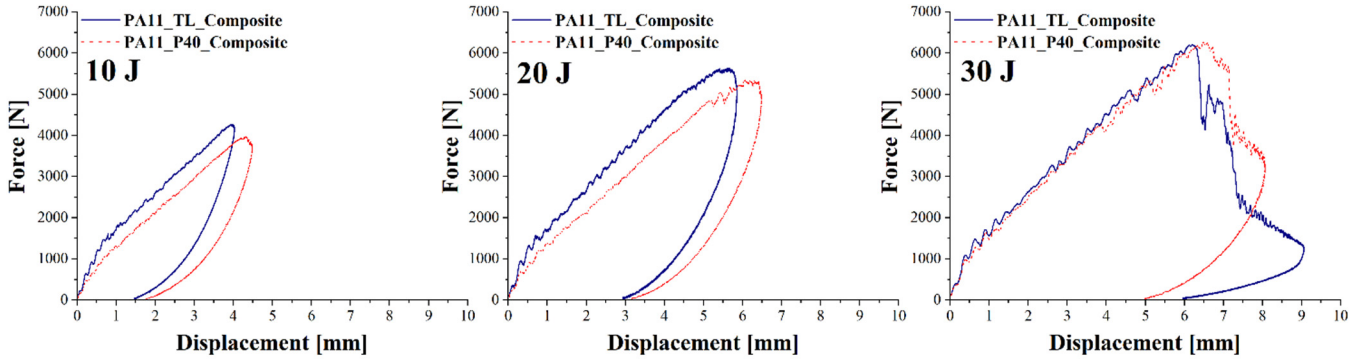

Figure 6. Representative impact response curves at room temperature of plasticized and non-plasticized PA11 composites.

These conclusions are corroborated by the damage visual inspection shown in Figure 7 and the profilometric analysis reported in Figure 8. Plasticized specimens experience a lower permanent indentation depth as a consequence of a more compliant response, thus displaying a higher damage tolerance. In particular, a decrease between 20.5% and 42.5% in permanent indentation can be observed at 10 J and 20 J, respectively. This confirms the effectiveness of the Butyl-Benzene-Sulfonamide plasticizer in improving the laminates' impact performance. The role of the plasticizer is crucial at room temperature because the PA11 matrix is working below its glass transition temperature, responding in a brittle way towards the impact. The absence of matrix plasticization phenomena prevents the absorption of a conspicuous amount of energy which is mainly dissipated through fiber and matrix breakage and eventually through delamination. Fiber breakage can be easily detected, for all impact energies, on the rear side of the composites, where a single straight crack running parallel to the basalt fibers can be observed. Crack direction distinctly underlines flax fibers failure, which takes place preferentially due to their lower tensile strength and the lower amount of energy required to break them. On the contrary, matrix cracking can be observed on the front side of the specimen, where many little cracks arise close to the area struck by the impactor and the clamped zone.

The results obtained are promising when compared with the ones reported in the literature for fully synthetic glass fiber/polypropylene (PP) composites [40–42]. In particular, Simeoli et al. [42] investigated PP composites reinforced with a glass woven fabric characterized by an average thickness of 3 mm and a fiber volume fraction of 50%, i.e., higher than the one used in this work, reporting comparable values of peak force, maximum displacement and absorbed energy. Zulkafli et al. [43] evaluated the impact response of PP laminates reinforced with glass fibers, banana fibers and their hybrid configurations. Their cross-ply composites with an average thickness of 3.3–3.6 mm were impacted at 102.5 J, and it was found that the hybrid configurations were characterized by a peak force between 2100 and 3970 N and absorbed energy between 10.7 and 20.2 J. These values are considerably lower than the ones achieved in the present work and can be conveniently compared with the 6600 N peak load and the 38.3 J absorbed energy reported by Zulkafli et al. for PP/glass fiber composite. Focusing on PA11 composites, the results obtained proved to be even more interesting. Lebaupin et al. [44] assessed the influence of stacking sequence, i.e., unidirectional, cross-ply, quasi-isotropic and sandwich-like, on the low-velocity impact response of flax reinforced PA11 composites with a fiber volume fraction of 0.50 and a thickness of 4 mm. Their results highlight a damage degree between 0.75 and 0.99, depending on composite configuration, after a 3.6 J impact. This damage degree is achieved at 20 J for the present work composite entailing a significant improvement in impact resistance. Furthermore, Vitiello et al. [45] evaluated the impact resistance of PA11/basalt composites with a fiber volume fraction of 0.45 and a thickness of 3 mm. Their composites display peak forces and maximum displacements comparable with the ones obtained in this work but are characterized by a damage degree almost 30–60% lower. This must be ascribed to

the intrinsic higher mechanical properties of basalt fibers over flax and the higher fiber volume fraction, i.e., 0.45 against 0.35 of the present work. According to Lebaupin et al. and Vitiello et al.'s findings, hybridization is clearly the perfect compromise to increase composite eco-friendliness and biodegradability while preserving impact resistance and is also a valid alternative to other synthetic configurations such as PP/glass fibers.

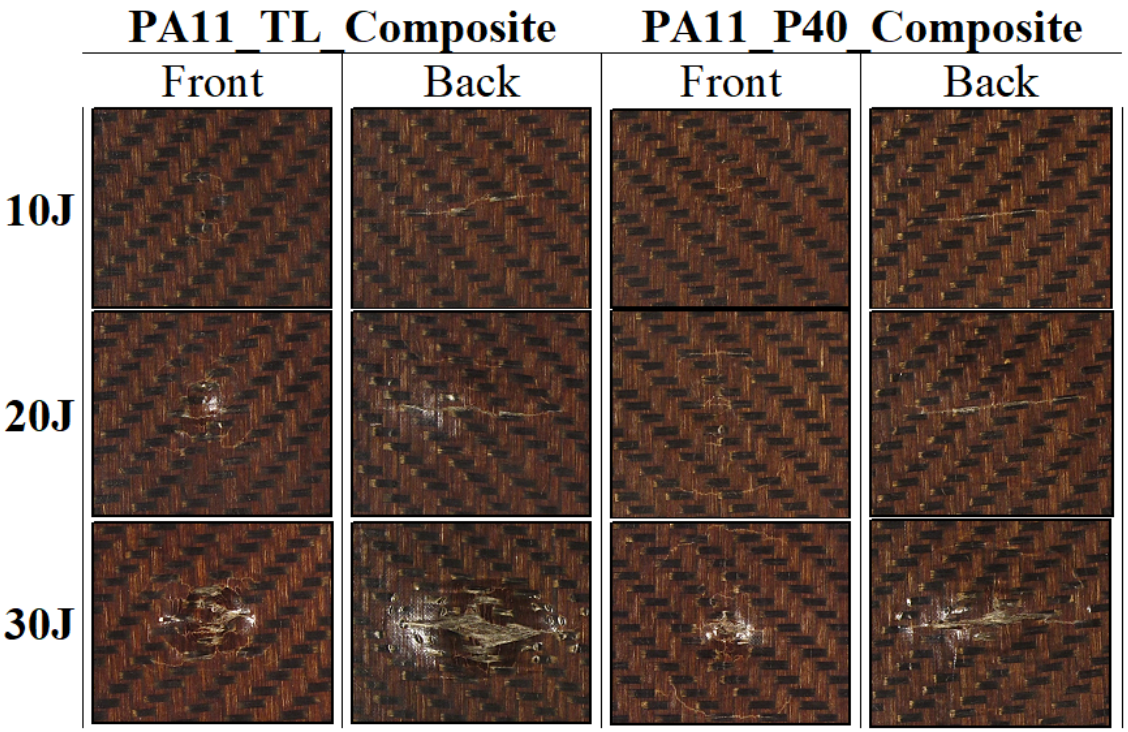

Figure 7. Damage progression as a function of impact energy at room temperature of plasticized and non-plasticized PA11 composites.

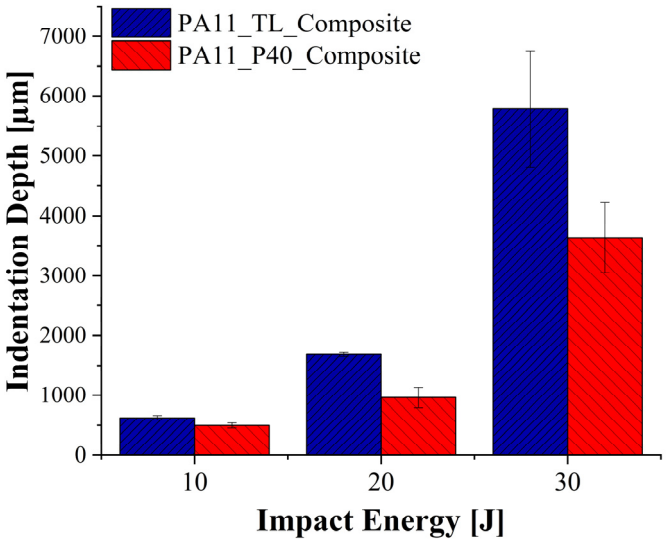

Figure 8. Permanent indentation depth at room temperature of plasticized and non-plasticized PA11 composites.

Some considerable differences can be observed in composites' response at +80 °C due to glass transition temperature crossing and matrix plasticization, as demonstrated by the impact curves reported in Figure 9 and the main impact parameters summarized in Figure 10. The transition from the glassy to the rubbery state causes a significant decrease

in laminates' stiffness which results in a substantial increase in maximum displacement and a considerable decrease in peak force. This change in deformation mode also affects the damage degree and damage mode, as confirmed by the permanent indentation data shown in Figure 11. In particular, an increase in absorbed energy, i.e., damage degree and permanent indentation, can be observed for both configurations at the lower impact energies. The activation of matrix plasticity makes the laminate more compliant toward the impact and allows it to dissipate a higher amount of energy while preserving the overall integrity. More specifically, in the glassy state, the material responds mainly elastically to the impact and all the energy absorbed is ascribed to matrix or fibers fracture. On the contrary, in the rubbery regime, matrix plasticization dissipates a considerable amount of impact energy, increasing the permanent indentation while preserving fiber integrity. The hypothesis of this additional energy dissipation mechanism is further confirmed by the observation of 30 J data. Looking at the impact curves at room temperature, both PA11_TL and PA11_P40 composites start to experience penetration, but none of them shows any sign of penetration when impacted at +80 °C. At room temperature, the approach of composite elastic limit and the brittle behavior of PA11 cause fibers breakage and a consequent steep increase in the permanent indentation and damage degree. On the contrary, the higher flexibility of PA11 at +80 °C allows us to control the damage degree and permanent indentation, keeping the laminate in the elastic regime. Similar results were reported by Sergi et al. [46], who studied the impact behavior of a polypropylene composite always reinforced with an intraply flax/basalt fabric in a wide range of temperatures, i.e., from −40 to +60 °C. In particular, Sergi et al. observed an increase of more than 20 J in laminate perforation energy moving from the glassy state at −40 °C to the rubbery regime at +60 °C with an undeniable improvement in composite's energy absorption capacity.

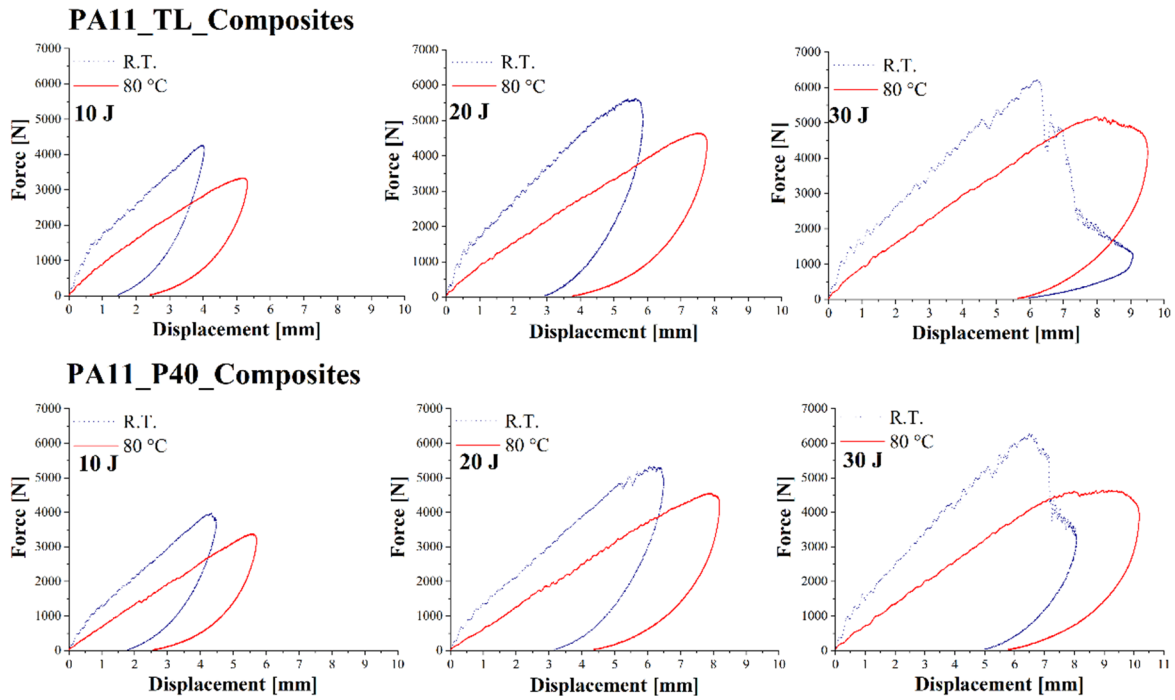

Figure 9. Representative impact response curves at room temperature and +80 °C of plasticized and non-plasticized PA11 composites.

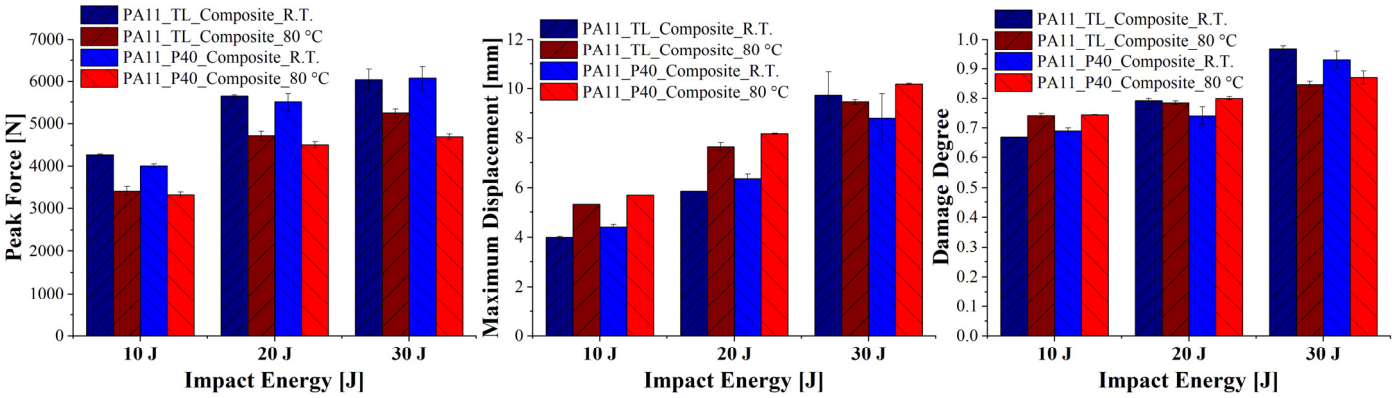

Figure 10. Main impact parameters, i.e., peak force, maximum displacement, and damage degree, of PA11 composites at room temperature and +80 °C.

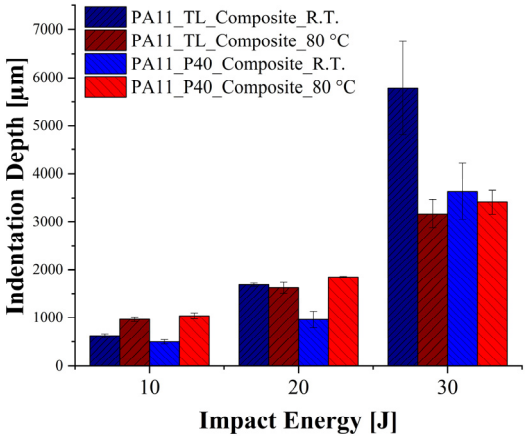

Figure 11. Permanent indentation depth at room temperature and at +80 °C of plasticized and non-plasticized PA11 composites.

A further consequence of the rubbery regime at +80 °C is the less pronounced effect of the plasticizer on the composite's impact response. In particular, the difference in damage degree and permanent indentation between PA11_TL and PA11_P40 becomes much less evident than at room temperature.

4. Conclusions

The effect of a Butyl-Benzene-Sulfonamide plasticizer on the impact response of a bio-polyamide PA11 reinforced with a hybrid flax/basalt woven fabric was assessed in this work. In addition, the effect of temperature on the impact behavior of these composite configurations was also evaluated. The main outcomes are:

- A decrease in melting and crystallization temperatures resulting from thermal analysis as a result of plasticizer introduction, with clear advantages in terms of processability and composite manufacturing.
- A reduction in the laminates' glass transition temperature as a consequence of hydrogen bond ruptures between amide groups, thus entailing the increased flexibility of the laminates.
- A great potential to replace traditional synthetic composites in terms of dynamic loading, displaying an impact response comparable to that of PP/glass fibers reported in the literature.
- A significant improvement in impact resistance with respect to PA11/flax composite and slightly lower performance than PA11/basalt laminates was reported in previous works, thus proving that hybridization is the best compromise between good mechanical properties and composite sustainability.

- Plasticizer addition provides a significant improvement in composite toughness, especially at room temperature, with a decrease in the permanent indentation and a delay of penetration phenomena fundamental to preserving the laminates' integrity and damage tolerance.
- The plasticizer effect is less prominent at +80 °C due to the matrix transition from a glassy to a rubbery state.

In conclusion, matrix plasticization with Butyl-Benzene-Sulfonamide is a suitable way to improve the impact resistance and toughness of PA11 Rilsan composites legitimating their application in the automotive sector, where they are already acknowledged as suitable materials for semi-structural purposes from the quasi-static performance perspective.

Author Contributions: Conceptualization, P.R., F.S. and J.T.; methodology, P.R., F.S. and J.T.; validation, C.S., F.S. and J.T.; formal analysis, P.R. and F.S.; investigation, L.V. and C.S.; resources, P.R., F.S. and J.T.; data curation, C.S.; writing—original draft preparation, C.S.; writing—review and editing, P.R., F.S. and J.T.; visualization, C.S.; supervision, P.R., F.S. and J.T. All authors have read and agreed to the published version of the manuscript.

Funding: This research received no external funding.

Institutional Review Board Statement: Not applicable.

Informed Consent Statement: Not applicable.

Data Availability Statement: Data are available within the article.

Conflicts of Interest: The authors declare no conflict of interest.

References

1. Plastic Europe; Association of Plastics Manufacturers. Plastics—The Facts 2021. An Analysis of European Plastics Production, Demand and Waste Data. 2021, p. 34. Available online: https://plasticseurope.org/knowledge-hub/plastics-the-facts-2021/ (accessed on 1 March 2022).
2. Market Research Report by Fortune Business Insights. In *Nylon Market Size by Type, by Application and Regional Forecast, 2020–2027*; Fortune Business Insights: Baner, India, 2020; p. 135. Available online: https://www.fortunebusinessinsights.com/nylon-market-102007 (accessed on 1 March 2022).
3. Winnacker, M.; Rieger, B. Biobased Polyamides: Recent Advances in Basic and Applied Research. *Macromol. Rapid Commun.* **2016**, *37*, 1391–1413. [CrossRef] [PubMed]
4. Armioun, S.; Pervaiz, M.; Sain, M. Biopolyamides and High-Performance Natural Fiber-Reinforced Biocomposites. In *Handbook of Composite from Renewable Materials*; Scrivener Publishing: Salem, MA, USA, 2017; Volume 3, pp. 253–270.
5. Holbery, J.; Houston, D. Natural-Fiber-Reinforced Polymer Composites in Automotive Applications. *JOM* **2006**, *58*, 80–86. [CrossRef]
6. Pickering, K.L.; Efendy, M.G.A.; Le, T.M. A review of recent developments in natural fibre composites and their mechanical performance. *Compos. Part A Appl. Sci. Manuf.* **2016**, *83*, 98–112. [CrossRef]
7. Boland, C.S.; De Kleine, R.; Keoleian, G.A.; Lee, E.C.; Kim, H.C.; Wallington, T.J. Life Cycle Impacts of Natural Fiber Composites for Automotive Applications: Effects of Renewable Energy Content and Lightweighting. *J. Ind. Ecol.* **2016**, *20*, 179–189. [CrossRef]
8. Li, M.; Pu, Y.; Thomas, V.M.; Yoo, C.G.; Ozcan, S.; Deng, Y.; Nelson, K.; Ragauskas, A.J. Recent advancements of plant-based natural fiber–reinforced composites and their applications. *Compos. Part B Eng.* **2020**, *200*, 108254. [CrossRef]
9. Faruk, O.; Bledzki, A.K.; Fink, H.P.; Sain, M. Biocomposites reinforced with natural fibers: 2000–2010. *Prog. Polym. Sci.* **2012**, *37*, 1552–1596. [CrossRef]
10. Huda, M.S.; Drzal, L.T.; Ray, D.; Mohanty, A.K.; Mishra, M. Natural-fiber composites in the automotive sector. In *Properties and Performance of Natural-Fibre Composites*; Pickering, K.L., Ed.; Woodhead Publishing: Sawston, UK, 2008; pp. 221–268. ISBN 9781845692674.
11. Shahzad, A. Hemp fiber and its composites—A review. *J. Compos. Mater.* **2012**, *46*, 973–986. [CrossRef]
12. Amico, S.C.; D'Almeida, J.R.M.; De Carvalho, L.H.; Cioffi, M.O.H. Hybrid Vegetable/Glass fiber composites. In *Lignocellulosic Polymer Composites: Processing, Characterization, and Properties*; Scrivener Publishing: Salem, MA, USA, 2014; pp. 63–81.
13. Nurazzi, N.M.; Asyraf, M.R.M.; Fatimah Athiyah, S.; Shazleen, S.S.; Ayu Rafiqah, S.; Harussani, M.M.; Kamarudin, S.H.; Razman, M.R.; Rahmah, M.; Zainudin, E.S.; et al. A review on mechanical performance of hybrid natural fiber polymer composites for structural applications. *Polymers* **2021**, *13*, 2170. [CrossRef]
14. Jawaid, M.; Abdul Khalil, H.P.S. Cellulosic/synthetic fibre reinforced polymer hybrid composites: A review. *Carbohydr. Polym.* **2011**, *86*, 1–18. [CrossRef]

15. Fiore, V.; Scalici, T.; Di Bella, G.; Valenza, A. A review on basalt fibre and its composites. *Compos. Part B Eng.* **2015**, *74*, 74–94. [CrossRef]
16. Boria, S.; Pavlovic, A.; Fragassa, C.; Santulli, C. Modeling of Falling Weight Impact Behavior of Hybrid Basalt/Flax Vinylester Composites. *Procedia Eng.* **2016**, *167*, 223–230. [CrossRef]
17. Zivkovi, I.; Fragassa, C.; Pavlovi, A.; Brugo, T. Influence of moisture absorption on the impact properties of flax, basalt and hybrid flax/basalt fiber reinforced green composites. *Compos. Part B* **2017**, *111*, 148–164. [CrossRef]
18. Almansour, F.A.; Dhakal, H.N.; Zhang, Z.Y. Investigation into Mode II interlaminar fracture toughness characteristics of flax/basalt reinforced vinyl ester hybrid composites. *Compos. Sci. Technol.* **2018**, *154*, 117–127. [CrossRef]
19. Prasath, K.A.; Krishnan, B.R. Mechanical Properties of Woven Fabric Basalt/Jute Fibre Reinforced Polymer Hybrid Composites. *Int. J. Mech. Eng. Robot. Res.* **2013**, *2*, 279–290.
20. Pandian, A.; Vairavan, M.; Winowlin, J.T.; Uthayakumar, M. Influence of stacking sequence on mechanical properties of basalt-jute fiber-reinforced polymer hybrid composites. *J. Polym. Eng.* **2012**, *32*, 547–554. [CrossRef]
21. Suresh Kumar, C.; Arumugam, V.; Dhakal, H.N.; John, R. Effect of temperature and hybridisation on the low velocity impact behavior of hemp-basalt/epoxy composites. *Compos. Struct.* **2015**, *125*, 407–416. [CrossRef]
22. Dhakal, H.N.; Sarasini, F.; Santulli, C.; Tirillò, J.; Zhang, Z.; Arumugam, V. Effect of basalt fibre hybridisation on post-impact mechanical behaviour of hemp fibre reinforced composites. *Compos. Part A Appl. Sci. Manuf.* **2015**, *75*, 54–67. [CrossRef]
23. Bazan, P.; Nosal, P.; Wierzbicka-Miernik, A.; Kuciel, S. A novel hybrid composites based on biopolyamide 10.10 with basalt/aramid fibers: Mechanical and thermal investigation. *Compos. Part B* **2021**, *223*, 109125. [CrossRef]
24. Armioun, S.; Panthapulakkal, S.; Scheel, J.; Tjong, J.; Sain, M. Biopolyamide hybrid composites for high performance applications. *J. Appl. Polym. Sci.* **2016**, *43595*, 1–9. [CrossRef]
25. Russo, P.; Simeoli, G.; Vitiello, L.; Filippone, G. Bio-Polyamide 11 Hybrid Composites Reinforced with Basalt/Flax Interwoven Fibers: A Tough Green Composite for Semi-Structural Applications. *Fibers* **2019**, *7*, 41. [CrossRef]
26. Oliver-Ortega, H.; Méndez, J.A.; Mutjé, P.; Tarrés, Q.; Espinach, F.X.; Ardanuy, M. Evaluation of thermal and thermomechanical behaviour of bio-based polyamide 11 based composites reinforced with lignocellulosic fibres. *Polymers* **2017**, *9*, 522. [CrossRef] [PubMed]
27. Ambrosio, J.D.; Balarim, C.V.M.; de Carvalho, G.B. Preparation, Characterization, and Mechanical/Tribological Properties of Polyamide11/Titanium Dioxide Nanocomposites. *Polym. Compos.* **2016**, *37*, 1415–1424. [CrossRef]
28. Adole, O.; Anguilano, L.; Minton, T.; Campbell, J.; Sean, L.; Valisios, S.; Tarverdi, K. Basalt fibre-reinforced high density polyethylene composite development using the twin screw extrusion process. *Polym. Test.* **2020**, *91*, 106467. [CrossRef]
29. Wang, S.; Zhong, J.; Gu, Y.; Li, G.; Cui, J. Mechanical properties, flame retardancy, and thermal stability of basalt fiber reinforced polypropylene composites. *Polym. Compos.* **2020**, *41*, 4181–4191. [CrossRef]
30. Kandemir, A.; Pozegic, T.R.; Hamerton, I.; Eichhorn, S.J.; Longana, M.L. Characterisation of natural fibres for sustainable discontinuous fibre composite materials. *Materials* **2020**, *13*, 2129. [CrossRef]
31. Kannan, T.G.; Wu, C.M.; Cheng, K.B.; Wang, C.Y. Effect of reinforcement on the mechanical and thermal properties of flax/polypropylene interwoven fabric composites. *J. Ind. Text.* **2013**, *42*, 417–433. [CrossRef]
32. Lafranche, E.; Oliveira, V.M.; Martins, C.I.; Krawczak, P. Prediction of injection-moulded flax fibre reinforced polypropylene tensile properties through a micro-morphology analysis. *J. Compos. Mater.* **2015**, *49*, 113–128. [CrossRef]
33. Xiao, X.; Cai, Z.; Qian, K. Structure evolution of polyamide (11)'s crystalline phase under uniaxial stretching and increasing temperature. *J. Polym. Res.* **2017**, *24*, 81. [CrossRef]
34. Ricou, P.; Pinel, E.; Juhasz, N. Temperature Experiments for Improved Accuracy in the Calculation of Polyamide-11 Crystallinity By X-ray Diffraction. *Denver X-ray Conf. Appl. X-ray Anal.* **2005**, *48*, 170–175.
35. Tey, W.S.; Cai, C.; Zhou, K. A Comprehensive Investigation on 3D Printing of Polyamide 11 and Thermoplastic Polyurethane via Multi Jet Fusion. *Polymers* **2021**, *13*, 2139. [CrossRef]
36. Latko, P.; Kolbuk, D.; Kozera, R.; Boczkowska, A. Microstructural Characterization and Mechanical Properties of PA11 Nanocomposite Fibers. *J. Mater. Eng. Perform.* **2016**, *25*, 68–75. [CrossRef]
37. Terinte, N.; Ibbett, R.; Schuster, K.C. Overview on native cellulose and microcrystalline cellulose I structure studied by X-ray diffraction (WAXD): Comparison between measurement techniques. *Lenzing. Ber.* **2011**, *89*, 118–131.
38. De Groote, P.; Rouxhet, P.; Devaux, J.; Godard, P. Infrared Study of the Hydrogen Bonding Association in Polyamides Plasticized by Benzenesulfonamides. Part I: Self-Association in Amide and Sulfonamide Systems; Part II: Amide–Sulfonamide Interaction. *Appl. Spectrosc.* **2001**, *55*, 877–887. [CrossRef]
39. De Groote, P.; Devaux, J.; Godard, P. The effect of benzenesulfonamide plasticizers on the glass transition temperature of an amorphous aliphatic polyamide. *Polym. Int.* **2002**, *51*, 40–49. [CrossRef]
40. Trudel-Boucher, D.; Bureau, M.N.; Denault, J.; Fisa, B. Low-Velocity Impacts in Continuous Glass Fiber/Polypropylene Composites. *Polym. Compos.* **2003**, *24*, 499–511. [CrossRef]
41. Zhao, Z.; Yang, Z.; Zhang, W.; Liu, D.; Li, Y.; Chen, J. Low-velocity impact response and infrared radiation characteristics of thermoplastic/thermoset composites. *Chin. J. Aeronaut.* 2022, *in press*. [CrossRef]
42. Simeoli, G.; Acierno, D.; Meola, C.; Sorrentino, L.; Iannace, S.; Russo, P. The role of interface strength on the low velocity impact behaviour of PP/glass fibre laminates. *Compos. Part B Eng.* **2014**, *62*, 88–96. [CrossRef]

43. Zulkafli, N.; Malingam, S.D.; Sheikh Md Fadzullah, S.H.; Razali, N. Quasi and dynamic impact performance of hybrid cross-ply banana/glass fibre reinforced polypropylene composites. *Mater. Res. Express* **2019**, *6*, 125344. [CrossRef]
44. Lebaupin, Y.; Hoang, T.T.; Chauvin, M.; Touchard, F. Influence of the stacking sequence on the low-energy impact resistance of flax / PA11 composite. *J. Compos. Mater.* **2019**, *53*, 3187–3198. [CrossRef]
45. Vitiello, L.; Russo, P.; Papa, I.; Lopresto, V.; Mocerino, D.; Filippone, G. Flexural properties and low-velocity impact behavior of polyamide 11/basalt fiber fabric laminates. *Polymers* **2021**, *13*, 1055. [CrossRef]
46. Sergi, C.; Sarasini, F.; Russo, P.; Vitiello, L.; Barbero, E.; Sanchez-Saez, S.; Tirillò, J. Effect of temperature on the low-velocity impact response of environmentally friendly cork sandwich structures. *J. Sandw. Struct. Mater.* **2022**, *24*, 1099–1121. [CrossRef]